Article:

Karageorghis, A, Bin-Mohsin, B, Lesnic, D et al. (1 more author) (2014) Simultaneous numerical determination of a corroded boundary and its admittance. Inverse Problems in Science and Engineering, 23 (7). 1120 - 1137. ISSN 1741-5977

https://doi.org/10.1080/17415977.2014.969728

SIMULTANEOUS NUMERICAL DETERMINATION OF A CORRODED BOUNDARY AND ITS ADMITTANCE

A. KARAGEORGHIS, B. BIN-MOHSIN, D. LESNIC, AND L. MARIN

Abstract. In this paper, an inverse geometric problem for Laplace's equation arising in boundary corrosion detection is considered. This problem, which consists of determining an unknown corroded portion of the boundary of a bounded domain and its admittance Robin coefficient from two pairs of boundary Cauchy data (boundary temperature and heat flux), is solved numerically using the meshless method of fundamental solutions. A nonlinear minimisation of the objective function is regularised, and the stability of the numerical results is investigated with respect to noise in the input data and various values of the regularisation parameters involved.

1. Introduction

When surfaces of a specimen which have been damaged by a corrosion aggressive attack are not accessible to direct inspection, one is forced to rely on overdetermined non-invasive measurements performed on the accessible part of the boundary. In this study, we consider such a non-destructive inspection technique modelled as an inverse geometric problem which consists of determining an unknown part of the boundary $\Gamma_2 \subset \partial\Omega$ assuming that the dependent variable (electric potential or steady-state temperature) u satisfies the Laplace equation in a simply-connected bounded domain Ω, namely

$$\Delta u = 0, \quad \text{in} \quad \Omega, \tag{1.1}$$

from the knowledge of the Dirichlet boundary data u and the Neumann flux data $\partial u/\partial n$, i.e. Cauchy data, on a known part of the boundary $\Gamma_1 = \partial\Omega \setminus \Gamma_2$, where $\boldsymbol{n}$ is the outward unit normal to the boundary, together with a Robin boundary condition on the unknown part of the boundary Γ_2 whose Robin coupling coefficient, called herein admittance, is also treated as unknown. A similar inverse problem arises from the non-destructive evaluation of the metal-to-silicon non-perfect interface in semiconductor devices [25].

Prior to this study, there were recent applications of the method of fundamental solutions (MFS) to solving the inverse boundary corrosion problem in electrostatics, [26, 28, 29, 32, 37], but the unknown boundary was restricted to be either perfectly conducting or insulated. In the case that a Robin convective boundary condition applies, the uniqueness of Γ_2 no longer holds and more measurements are necessary.

The inverse, nonlinear and ill-posed problem of determining the unknown (inaccessible) corroded portion of the boundary Γ_2 and its admittance coefficient is approached using a regularised minimisation procedure which employs the MFS. We mention that the analogous inverse corrosion problem in heat transfer governed by the modified Helmholtz equation was recently solved numerically in [3]. However, in comparison with other related works on the subject of simultaneous determination of a corroded boundary and its Robin coefficient, [3, 10, 24], the present study contributes as follows. Firstly, we employ a flexible dynamic pseudo-boundary MFS approach which allows for the distance between the boundary and the fictitious curve on which the source are positioned to be optimised. This approach has recently been proved to be successful in related applications of the MFS for solving shape identification problems in both two and three dimensions, [20, 21]. Secondly, the nonlinear minimization is performed using the MATLAB© [31] optimization toolbox routine `lsqnonlin`. In contrast to the more classical

Date: June 12, 2014.
2000 *Mathematics Subject Classification.* Primary 65N35; Secondary 65N21, 65N38.
Key words and phrases. Laplace's equation; Inverse problem; Method of fundamental solutions; Regularisation.

Fortran NAG [33] routines, e.g. `E04FCF`, which do not require the gradient of the objective function to be supplied by the user, the routine `lsqnonlin` allows simple bounds on the unknown variables to be imposed. This is particularly useful and important because we know beforehand that certain physical or geometrical quantities are positive for example. There exist other NAG routines that allow the user to supply bounds on the unknowns, e. g. `E04UCF`, `E04UNF`. However, these require the user to provide as many components of the gradient of the objective functional as possible and, most importantly, they are computationally very expensive. The outline of this paper is as follows. In section 2 we introduce and discuss the mathematical formulation, whilst in section 3 we present the regularised MFS for the solving the inverse problem. In section 4 we present and discuss the numerically obtained results, whilst section 5 gives conclusions and possible future work.

2. Mathematical formulation

We consider that the solution domain Ω is simply-connected and bounded by a piecewise smooth curve $\partial\Omega$, such that $\partial\Omega = \Gamma_1 \cup \Gamma_2$, $\Gamma_1 \cap \Gamma_2 = \emptyset$, and Γ_1 and Γ_2 are of positive measure without cusps at the intersection $\overline{\Gamma}_1 \cap \overline{\Gamma}_2$. The function u satisfies the Laplace equation (1.1) subject to the boundary conditions

$$u = f \qquad \text{on} \quad \Gamma_1, \tag{2.1}$$

and

$$\frac{\partial u}{\partial n} + \alpha u = 0 \qquad \text{on} \quad \Gamma_2, \tag{2.2}$$

where $f \in H^{1/2}(\partial\Omega)$ is a given non-constant function and $\alpha \in L^\infty(\Gamma_2)$ is the non-negative surface admittance in electrostatics, or the surface heat transfer coefficient in heat conduction. In equations (1.1) and (2.2) we have assumed that, for simplicity, the conductivity is constant and equal to unity. Here $H^{1/2}(\partial\Omega)$ denotes the space of traces of functions $u \in H^1(\Omega)$ restricted to the boundary $\partial\Omega$, and $H^{-1/2}(\partial\Omega)$ denotes the dual space of $H^{1/2}(\partial\Omega)$. Equation (2.2) represents a homogeneous Robin boundary condition and, based on Newton's law of cooling, it expresses that the ambient effects (thermal or electrostatic) are uniform and, for simplicity, taken to be zero. We mention that in some papers the admittance is often called impedance and although there is some physical distinction between them, e.g. one is the reciprocal of the other, mathematically this is equivalent as we can always rewrite equation (2.2) as $\alpha^{-1}\partial u/\partial n + u = 0$.

It is well-known that the direct Dirichlet-Robin problem given by equations (1.1), (2.1) and (2.2) has a unique solution $u \in H^1(\Omega)$, when Γ_2 is known. Since we want to use non-destructive testing, we then define a nonlinear operator which maps the set of admissible C^1-corroded boundary Γ_2 with admittance $\alpha \in L^\infty(\Gamma_2)$, $\alpha \geqslant 0$, to the data space of Neumann flux in $H^{-1/2}(\Gamma_1)$, as follows:

$$F_f(\Gamma_2, \alpha) := \frac{\partial u}{\partial n}\Big|_{\Gamma_1} = g \in H^{-1/2}(\Gamma_1). \tag{2.3}$$

In the inverse boundary corrosion problem setting, [22], Γ_2 is some unknown and inaccessible corroded boundary portion of $\partial\Omega$, whilst Γ_1 is known and accessible for input-output measurements, i.e. Cauchy data prescription. Then the inverse problem under consideration consists of extracting some information about the boundary Γ_2 and its admittance α from a couple of data $g_1 = F_{f_1}(\Gamma_2, \alpha)$ and $g_2 = F_{f_2}(\Gamma_2, \alpha)$. The data (2.3) may also be only partial, i.e. the flux being measured on a non-zero measure portion $\Gamma \subset \Gamma_1$, instead of the whole boundary Γ_1. It is well-known that this inverse problem is nonlinear and ill-posed, as opposed to the direct problem which is linear and well-posed.

We briefly note that the situation regarding the uniqueness/non-uniqueness of solution is much more settled in the case of the inverse shape boundary determination of Γ_2 when α is known, [6, 7, 9, 17, 18], or in the case of the inverse admittance determination of α when Γ_2 is known, [11, 16]. We also mention that the case of the inverse determination of Γ_2 with α unknown but being either 0, i.e. a perfectly insulating boundary corrosion, or ∞, i.e. a perfectly conducting boundary corrosion, has recently been investigated in [30]. However, it is not always physically realistic to assume that the boundary condition on the corroded boundary is known, e.g. on a rough metal surface covered by a layer of a corrosive fluid, in which situation the coefficient α in (2.2) together with the boundary Γ_2 are to be simultaneously determined. Then, clearly one set of Cauchy boundary measurements (2.1) and (2.3) is not sufficient to simultaneously recover the boundary Γ_2 affected by a corrosion attack and its corrosion coefficient α. Even when α is known, one set of Cauchy data (2.1) and (2.3) may not be enough to determine uniquely the corroded boundary Γ_2, as shown by the counterexamples given in [7, 9, 35] and some thorough numerical investigation reported in [15]. However, it turns out that two linearly independent boundary data f_1 and f_2, one of which is positive, inducing, via (2.3), two corresponding flux measurements g_1 and g_2, are sufficient to provide a unique solution for the pair (Γ_2, α), [1, 34, 35]. The stability issue has also been recently addressed in [36] and numerical results based either on a potential approach or on a Green's integral formulation have been reported in [10].

Summing up, the mathematical formulation of the inverse problem under investigation requires determining the corroded boundary Γ_2, the admittance coefficient α, and the electrostatic potentials u_ℓ for $\ell = 1, 2$, satisfying the two-Cauchy data Robin problem

$$\Delta u_\ell = 0, \quad \text{in} \quad \Omega, \tag{2.4}$$

$$\frac{\partial u_\ell}{\partial n} + \alpha u_\ell = 0, \qquad \text{on} \quad \Gamma_2, \tag{2.5}$$

$$u_\ell = f_\ell, \qquad \text{on} \quad \Gamma_1, \tag{2.6}$$

$$\frac{\partial u_\ell}{\partial n} = g_\ell, \qquad \text{on} \quad \Gamma_1, \tag{2.7}$$

for $\ell = 1, 2$.

In the next section we describe the MFS and the nonlinear minimization employed for solving the inverse geometric problem (2.4)-(2.7).

3. The method of fundamental solutions (MFS)

For simplicity, we describe the analysis in two dimensions with the mention that the extension to three dimensions is reasonably straight-forward, but for a higher computational effort involved. In the application of the MFS to (2.4), we seek an approximation as a linear combination of fundamental solutions of the form [14]

$$u_N(\boldsymbol{c}, \boldsymbol{\xi}; \boldsymbol{x}) = \sum_{k=1}^{2N} c_k \, G(\boldsymbol{\xi}_k, \boldsymbol{x}), \quad \boldsymbol{x} \in \overline{\Omega}, \tag{3.1}$$

where $(\boldsymbol{\xi}_k)_{k=1}^{2N}$ are source points located outside $\overline{\Omega}$ and G is the fundamental solution of the two-dimensional Laplace equation, given by

$$G(\boldsymbol{\xi}, \boldsymbol{x}) = -\frac{1}{2\pi} \ln | \, \boldsymbol{\xi} - \boldsymbol{x} \, | \ . \tag{3.2}$$

Assume that Ω is a star-shaped domain with respect to the origin and has a smooth boundary $\partial\Omega$ parametrised by

$$\partial\Omega = \{r(\vartheta)(\cos(\vartheta), \sin(\vartheta)) | \, \vartheta \in [0, 2\pi)\}, \tag{3.3}$$

where $r(\vartheta)$ is a $2\pi-$periodic smooth function. We take the accessible part of the boundary

$$\Gamma_1 = \{r(\vartheta)(\cos\vartheta, \sin\vartheta) | \, \vartheta \in [0, \pi]\}\,, \tag{3.4}$$

where $r(\vartheta)$ is known for $\vartheta \in [0, \pi]$. We further assume that the corroded part of the boundary can be parametrised by

$$\Gamma_2 = \{r(\vartheta)(\cos\vartheta, \sin\vartheta) | \vartheta \in (\pi, 2\pi)\}\,, \tag{3.5}$$

where now $r(\vartheta)$ is *not* known for $\vartheta \in (\pi, 2\pi)$.

We choose the collocation points on Γ_1 to be

$$\boldsymbol{x}_k = r_k\left(\cos\vartheta_k, \sin\vartheta_k\right), \quad \vartheta_k = \frac{\pi(k-1)}{M}, \quad k = \overline{1, M+1}, \tag{3.6}$$

and the collocation points on Γ_2 to be

$$\boldsymbol{x}_k = r_k\left(\cos\vartheta_k, \sin\vartheta_k\right), \quad \vartheta_k = \pi + \frac{\pi(k-M-1)}{N}, \quad k = \overline{M+2, M+N}. \tag{3.7}$$

where $r_k = r(\vartheta_k)$, $k = \overline{1, M+N}$. The r_k, $k = \overline{1, M+1}$ are known, whereas the r_k, $k = \overline{M+2, M+N}$ are unknown. We further choose the source points corresponding to Γ_1 to be

$$\boldsymbol{\xi}_k = \eta\, r_k\left(\cos\phi_k, \sin\phi_k\right), \quad \phi_k = \frac{\pi(k-1)}{N}, \quad k = \overline{1, N+1}, \tag{3.8}$$

and the source points corresponding to Γ_2 to be

$$\boldsymbol{\xi}_\ell = \eta\, r_\ell\,\left(\cos\vartheta_\ell, \sin\vartheta_\ell\right), \quad \vartheta_\ell = \pi + \frac{\pi(\ell-N-1)}{N}, \quad \ell = \overline{N+2, 2N}, \tag{3.9}$$

where the (unknown) dilation parameter $\eta > 1$.

3.1. **Finite-dimensional parametrisation.** In order to improve the accuracy and stability of the numerical results, we introduce an additional finite-dimensional trigonometric polynomial approximations for Γ_2 and α, as [12],

$$r^K(\vartheta) = a_0 + \sum_{j=1}^{K} a_j \cos(j\vartheta) + \sum_{j=1}^{K} b_j \sin(j\vartheta), \qquad \vartheta \in (\pi, 2\pi), \tag{3.10}$$

$$\alpha_L(\vartheta) = C_0 + \sum_{j=1}^{L} C_j \cos(j\vartheta) + \sum_{j=1}^{L} D_j \sin(j\vartheta), \qquad \vartheta \in (\pi, 2\pi). \tag{3.11}$$

Alternatively, cubic B-splines can also be used, [15], in place of the trigonometric approximation (3.10).

3.2. **Nonlinear Minimization.** In the application of the MFS to the inverse problem (2.4)-(2.7), there are now $4N+2K+2L+2$ unknowns consisting of the $4N$ coefficients $\left(c_k^\ell\right)_{k=\overline{1,2N}}$, $\ell = 1, 2$, in (3.1), the $2K+1$ coefficients in (3.10), the $2L+1$ coefficients in (3.11) and the dilation coefficient η in (3.9). These can be determined by imposing the boundary conditions (2.5)-(2.7) in a least-squares sense. This leads to the minimization of the functional

$$\begin{aligned} S(\boldsymbol{c}^1, \boldsymbol{c}^2, \boldsymbol{r}, \boldsymbol{\alpha}, \eta) := {} & \textstyle\sum_{\ell=1}^{2}\sum_{j=1}^{M+1}\left[u_{\ell_N}(\boldsymbol{c}^\ell, \boldsymbol{\xi}; \boldsymbol{x}_j) - f_\ell(\boldsymbol{x}_j)\right]^2 + \sum_{\ell=1}^{2}\sum_{j=1}^{M+1}\left[\dfrac{\partial u_{\ell_N}}{\partial n}(\boldsymbol{c}^\ell, \boldsymbol{\xi}; \boldsymbol{x}_j) - g_\ell^\varepsilon(\boldsymbol{x}_j)\right]^2 \\ & + \textstyle\sum_{\ell=1}^{2}\sum_{j=2}^{N}\left[\dfrac{\partial u_{\ell_N}}{\partial n}(\boldsymbol{c}^\ell, \boldsymbol{\xi}; \boldsymbol{x}_{M+1+j}) + \alpha u_{\ell_N}(\boldsymbol{c}, \boldsymbol{\xi}; \boldsymbol{x}_{M+1+j})\right]^2 \\ & + \left[a_0 + \textstyle\sum_{j=1}^{K} a_j - r(0)\right]^2 + \left[a_0 + \sum_{j=1}^{K}(-1)^j a_j - r(\pi)\right]^2, \end{aligned} \tag{3.12}$$

where $\boldsymbol{c}^\ell = [c_1^\ell, c_2^\ell, \ldots, c_{2N}^\ell]$, $\ell = 1, 2$, $\boldsymbol{r} = [a_0, a_1, \ldots a_K, b_1, \ldots, b_K]$ and $\boldsymbol{\alpha} = [C_0, C_1, \ldots C_L, D_1, \ldots, D_L]$.
Note that the last two terms in (3.12) correspond to the specification of $r(0)$ and $r(\pi)$ such that there is no discontinuity at the intersection points of $\overline{\Gamma}_1 \cap \overline{\Gamma}_1$.
The functional S in (3.12) imposes $2N + 4M + 4$ conditions and we thus require $2N + 4M + 4 \geq 4N + 2K + 2L + 2$ or $2M \geq N + K + L - 1$. It is easy to imagine how functional (3.12) can be generalized, through the MFS formulation, to naturally incorporate additional Cauchy data should multiple, say more than two, sets of independent measurements become available to yield more information and hence even better reconstructions of the unknown corroded boundary Γ_2, its admittance coefficient α, and possibly other additional parameters, see e.g. [4].

Remarks.

(i) The flux data (2.7) comes from practical measurements which is inherently contaminated with noisy errors, and therefore we replace g_l by g_l^ϵ given by

$$g_l^\epsilon(\boldsymbol{x}_j) = (1+\rho_j p) g_l(\boldsymbol{x}_j), \quad j = \overline{1,(M+1)}, \tag{3.13}$$

where p represents the percentage of noise and ρ_j is a pseudo-random noisy variable drawn from a uniform distribution in $[-1,1]$ using the MATLAB© command `-1+2*rand(1,M)`.

(ii) Since the inverse problem is ill-posed, in order to achieve the stability of the numerical MFS solution for noisy data (2.7), in (3.12), we can add the regularization terms

$$\lambda_1\left(|\boldsymbol{c}^1|^2 + |\boldsymbol{c}^2|^2\right) + \lambda_2\Big(\sum_{j=0}^{K} a_j^2 + \sum_{j=1}^{K} b_j^2\Big) + \lambda_3\Big(\sum_{j=0}^{L} C_j^2 + \sum_{j=1}^{L} D_j^2\Big) \tag{3.14}$$

where $\lambda_1, \lambda_2, \lambda_3 \geq 0$ are regularization parameters to be prescribed.

(iii) In (3.12), the outward normal vector $\boldsymbol{n}$ is defined as follows:

$$\boldsymbol{n}(\vartheta) = \frac{1}{\sqrt{r^2(\vartheta) + r'^2(\vartheta)}}\left[(r'(\vartheta)\sin\vartheta + r(\vartheta)\cos\vartheta)\,\boldsymbol{i} - (r'(\vartheta)\cos\vartheta - r(\vartheta)\sin\vartheta)\,\boldsymbol{j}\right], \tag{3.15}$$

where $\boldsymbol{i} = (1,0)$ and $\boldsymbol{j} = (0,1)$. As a result, from (3.1) the normal derivative $\partial_n u_N$ is evaluated as

$$\partial_n u_N = \boldsymbol{n} \cdot \nabla u_N = -\frac{1}{2\pi}\sum_{k=1}^{2N} c_k \frac{(\boldsymbol{x} - \boldsymbol{\xi}_k)\cdot \boldsymbol{n}}{|\boldsymbol{x} - \boldsymbol{\xi}_k|^2}. \tag{3.16}$$

In (3.15), for the unknown part of the boundary Γ_2, we use

$$r'(\vartheta) = -\sum_{j=1}^{K} j a_j \sin(j\vartheta) + \sum_{j=1}^{K} j b_j \cos(j\vartheta), \qquad \vartheta \in (\pi, 2\pi), \tag{3.17}$$

while for the known part of the boundary Γ_1, we simply calculate the derivative $r'(\vartheta)$ since we know the expansion of $r(\vartheta)$ there.

(iv) The minimization of functional (3.12) is carried out using the MATLAB© optimization toolbox routine `lsqnonlin` which solves nonlinear least squares problems. The routine `lsqnonlin` does not require the user to provide the gradient and, in addition, it offers the option of imposing lower and upper bounds on the elements of the vector of unknowns $(\boldsymbol{c}^1, \boldsymbol{c}^2, \boldsymbol{r}, \boldsymbol{\alpha}, \eta)$ through the vectors `lb` and `up`.

4. Numerical examples

4.1. **Construction of appropriate harmonic functions.** Suppose that we now consider the general curve $r(\vartheta)$ and want to construct a harmonic function u satisfying the homogeneous Robin condition (2.2) on the lower boundary Γ_2. We first remark that because of the singularities of the solution of the direct Dirichlet-Robin problem (1.1), (2.1) and (2.2) at the two intersection points $\overline{\Gamma}_1 \cap \overline{\Gamma}_2$, any numerical method discretizing/collocating boundaries (3.4) and (3.5) with equidistant points on $[0, 2\pi)$ will lead to inaccuracies. A graded mesh towards the intersection points may be employed as in [23], but in this section a simpler construction method of appropriate harmonic functions is proposed to fit our purpose of generating accurate numerically simulated data (2.6) and (2.7). For given $\mathcal{A}, \mathcal{B}, \mathcal{C}$, consider the harmonic function

$$u(r,\vartheta) = \mathcal{A} + \mathcal{B} r\cos\vartheta + \mathcal{C} r\sin\vartheta + \sum_{\ell=2}^{\mathcal{L}} r^\ell\left[A_\ell\,\cos(\ell\vartheta) + B_\ell\,\sin(\ell\vartheta)\right], \tag{4.1}$$

for a fixed $\mathcal{L} \in \mathbb{N}^*$.

Then

$$\frac{\partial u}{\partial r}(r,\vartheta) = \mathcal{B}\cos\vartheta + \mathcal{C}\sin\vartheta + \sum_{\ell=2}^{\mathcal{L}} \ell r^{\ell-1}\left[A_\ell\,\cos(\ell\vartheta) + B_\ell\,\sin(\ell\vartheta)\right], \tag{4.2}$$

and

$$\frac{\partial u}{\partial \vartheta}(r,\vartheta) = -\mathcal{B}r\sin\vartheta + \mathcal{C}r\cos\vartheta + \sum_{\ell=2}^{\mathcal{L}} \ell r^{\ell}\left[-A_\ell\,\sin(\ell\vartheta) + B_\ell\,\cos(\ell\vartheta)\right]. \tag{4.3}$$

We can now find the normal derivative on the boundary from

$$\frac{\partial u}{\partial n}(r,\vartheta) = n_x\frac{\partial u}{\partial x} + n_y\frac{\partial u}{\partial y} = \left[\cos\vartheta\frac{\partial u}{\partial r} - \frac{\sin\vartheta}{r}\frac{\partial u}{\partial \vartheta}\right]n_x + \left[\sin\vartheta\frac{\partial u}{\partial r} + \frac{\cos\vartheta}{r}\frac{\partial u}{\partial \vartheta}\right]n_y, \tag{4.4}$$

where from (3.15),

$$n_x(\vartheta) = \frac{1}{\sqrt{r^2(\vartheta)+r'^2(\vartheta)}}\left(r'(\vartheta)\sin\vartheta + r(\vartheta)\cos\vartheta\right), \quad n_y(\vartheta) = -\frac{1}{\sqrt{r^2(\vartheta)+r'^2(\vartheta)}}\left(r'(\vartheta)\cos\vartheta - r(\vartheta)\sin\vartheta\right). \tag{4.5}$$

After some manipulations we obtain that

$$\begin{aligned}\frac{\partial u}{\partial n}(r,\vartheta) = &\left\{\mathcal{B} + \sum_{\ell=2}^{\mathcal{L}} \ell r^{\ell-1}\left[A_\ell\cos((\ell-1)\vartheta) + B_\ell\sin((\ell-1)\vartheta)\right]\right\}n_x\\ &+\left\{\mathcal{C} + \sum_{\ell=2}^{\mathcal{L}} \ell r^{\ell-1}\left[-A_\ell\sin((\ell-1)\vartheta) + B_\ell\cos((\ell-1)\vartheta)\right]\right\}n_y.\end{aligned} \tag{4.6}$$

The boundary condition $\dfrac{\partial u}{\partial n} + \alpha u = 0$ thus becomes

$$\begin{aligned}&\sum_{\ell=2}^{\mathcal{L}}\left\{\ell r^{\ell-1}\left[\cos((\ell-1)\vartheta)n_x(\vartheta) - \sin((\ell-1)\vartheta)n_y(\vartheta)\right] + \alpha(\vartheta)r^\ell\cos(\ell\vartheta)\right\}A_\ell\\ &+\sum_{\ell=2}^{\mathcal{L}}\left\{\ell r^{\ell-1}\left[\sin((\ell-1)\vartheta)n_x(\vartheta) + \cos((\ell-1)\vartheta)n_y(\vartheta)\right] + \alpha(\vartheta)r^\ell\sin(\ell\vartheta)\right\}B_\ell\\ &\qquad= -\mathcal{B}n_x(\vartheta) - \mathcal{C}n_y(\vartheta) - \alpha(\vartheta)\left(\mathcal{A} + \mathcal{B}r\cos\vartheta + \mathcal{C}r\sin\vartheta\right).\end{aligned} \tag{4.7}$$

The $2(\mathcal{L}-1)$ coefficients $(A_\ell)_{\ell=2}^{\mathcal{L}}$ and $(B_\ell)_{\ell=2}^{\mathcal{L}}$ can be determined by collocating equation (4.7) at the $\mathcal{M}-1$ points $\tilde{\vartheta}_i = \pi + \frac{i}{\mathcal{M}}$, $i = 1,\dots,\mathcal{M}-1$. Taking $\mathcal{M} \geq 2\mathcal{L}-1$ this yields the overdetermined system of linear equations

$$\begin{aligned}&\sum_{\ell=2}^{\mathcal{L}}\left\{\ell r_i^{\ell-1}\left[\cos((\ell-1)\tilde{\vartheta}_i)n_x(\tilde{\vartheta}_i) - \sin((\ell-1)\tilde{\vartheta}_i)n_y(\tilde{\vartheta}_i)\right] + \alpha(\tilde{\vartheta}_i)r_i^\ell\cos(\ell\tilde{\vartheta}_i)\right\}A_\ell\\ &+\sum_{\ell=2}^{\mathcal{L}}\left\{\ell r_i^{\ell-1}\left[\sin((\ell-1)\tilde{\vartheta}_i)n_x(\tilde{\vartheta}_i) + \cos((\ell-1)\tilde{\vartheta}_i)n_y(\tilde{\vartheta}_i)\right] + \alpha(\tilde{\vartheta}_i)r_i^\ell\sin(\ell\tilde{\vartheta}_i)\right\}B_\ell\\ &= -\mathcal{B}n_x(\tilde{\vartheta}_i) - \mathcal{C}n_y(\tilde{\vartheta}_i) - \alpha(\tilde{\vartheta}_i)\left(\mathcal{A} + \mathcal{B}r_i\cos\tilde{\vartheta}_i + \mathcal{C}r_i\sin\tilde{\vartheta}_i\right), \quad i = 1,\dots,\mathcal{M}-1,\end{aligned} \tag{4.8}$$

where $r_i = r(\tilde{\vartheta}_i)$.

Having determined the coefficients $(A_\ell)_{\ell=2}^{\mathcal{L}}$, $(B_\ell)_{\ell=2}^{\mathcal{L}}$ we can then calculate from (4.1) the Cauchy data on Γ_1.

4.2. **Example 1.** In this example, the unit disk domain $\Omega = B(\mathbf{0};1)$ is considered, and its boundary is divided into two parts, namely,

$$\Gamma_1 = \{(x,y) \in \mathbb{R}^2 |\ x = \cos(\vartheta);\ y = \sin(\vartheta);\ \vartheta \in [0,\pi]\}, \tag{4.9}$$

and

$$\Gamma_2 = \{(x,y) \in \mathbb{R}^2 |\ x = r(\vartheta)\cos(\vartheta);\ y = r(\vartheta)\sin(\vartheta);\ \vartheta \in (\pi,2\pi), r(\vartheta) = 1\}. \tag{4.10}$$

First, we take the Dirichlet data (2.1) on Γ_1 given by

$$u_1(1,\vartheta) = f_1(\vartheta) = \mathrm{e}^{\gamma\sin(\vartheta)}\cos\big(\gamma\cos(\vartheta)\big), \qquad \vartheta \in [0,\pi], \tag{4.11}$$

where $\gamma = \pi/4$, and the Neumann data (2.3) on Γ_1 given by

$$\frac{\partial u_1}{\partial n}(1,\vartheta) = \frac{\partial u_1}{\partial r}(1,\vartheta) = g_1(\vartheta) = \gamma\mathrm{e}^{\gamma\sin(\vartheta)}\sin\big(\vartheta - \gamma\cos(\vartheta)\big), \qquad \vartheta \in [0,\pi]. \tag{4.12}$$

We also take the positive Robin coefficient given by

$$\alpha(\vartheta) = -\frac{\gamma\sin\big(\vartheta - \gamma\cos(\vartheta)\big)}{\cos\big(\gamma\cos(\vartheta)\big)}, \qquad \vartheta \in (\pi,2\pi). \tag{4.13}$$

Graphs of the Dirichlet data (4.11) and the Robin coefficient (4.13) are presented in Figures 1(a) and 2(b), respectively, showing that they are positive.
Note that the analytical solution of the direct problem (1.1), (2.1) and (2.2) with the data given by (4.9)-(4.11) and (4.13) is given by

$$u_1(r,\vartheta) = e^{\gamma r\sin(\vartheta)}\cos\big(\gamma r\cos(\vartheta)\big), \quad (r,\vartheta) \in \Omega. \tag{4.14}$$

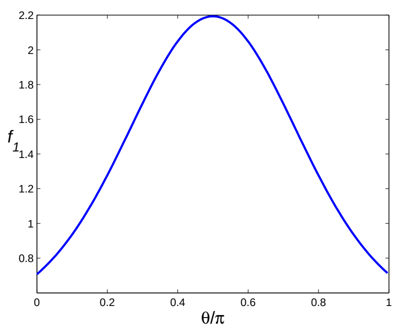

(a)

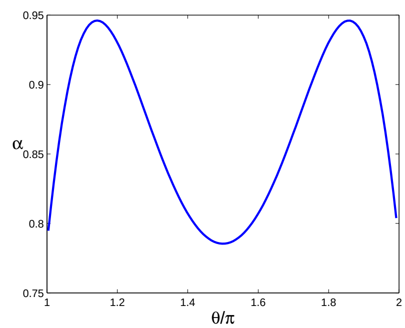

(b)

FIGURE 1. (a) The Dirichlet boundary data (4.11) and (b) the Robin coefficient (4.13) for $\gamma = \pi/4$.

We also need a second set of Cauchy data (2.1) and (2.3) on Γ_1 linearly independent of (4.11) and (4.12). We generate such a function u_2 given from (4.1) with $\mathcal{A} = \mathcal{B} = \mathcal{C} = 1$ and $\mathcal{L} = 8$. The unknown coefficients $(A_\ell)_{\ell=2}^{8}$, $(B_\ell)_{\ell=2}^{8}$ are determined by collocating equation (4.8) with $\mathcal{M} = 800$.
In the inverse problem, both the corroded boundary Γ_2 and its admittance coefficient α are unknown. In order to ensure the uniqueness of solution we combine the Cauchy data (4.11), (4.12) and those in Figure 2 on Γ_1. These Dirichlet boundary data are linearly independent with at least one of them positive, see Figure 1(a). Further, the way in which this data has been generated (one analytically and the other one using a Trefftz-type search) clearly avoids committing an inverse crime because the inverse solver is based on a nonlinear iterative minimization. We take $K = 3$ and $L = 3$ in (3.10) and (3.11), respectively. As initial guesses for the iterative nonlinear minimization of the objective functional (3.12), we take $a_0 = 1, b_1 = 0.5$ and all other coefficients to be zero in (3.10), while in (3.11) we take $C_0 = 0.85$ and all other coefficients are be equal to zero, and $\eta_0 = 1.1$.

In the subsequent Figures 3-6, 9-11 and 13-14 where we present Γ_2 and α, the initial guess, the numerical reconstruction and the exact solution are shown in blue ($---$), in red ($\cdots$) and in black ($-$), respectively. We first consider the case of no noise and no regularization. In Figure 3(a) we present the initial guess and numerically reconstructed boundary Γ_2 with $M = 80, N = 40$ for various numbers of iterations. We also take the initial guesses for the MFS coefficients $\boldsymbol{c}^1$ and $\boldsymbol{c}^2$ to be zero. The corresponding results for the admittance coefficient α are presented in Figure 3(b). The results with the same initial parameters but with $M = 100, N = 50$ are presented in Figure 4. From both Figures 3(a) and 4(a) it can be seen that the semi-circular lower boundary (3.5) is very accurately retrieved in less than 100 iterations. Furthermore, by comparing Figures 3(b) and 4(b) it can be seen that the accuracy in the retrieved admittance coefficient increases as M and N increase.

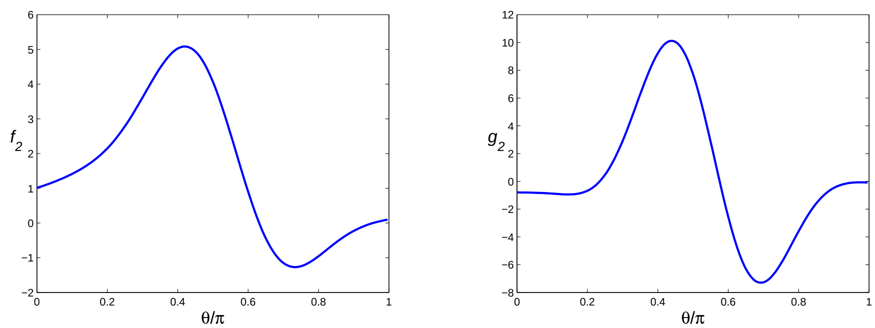

(a) (b)

FIGURE 2. Example 1: (a) The Dirichlet boundary data (2.6), and (b) the Neumann boundary data (2.7) determined from the system of equations (4.8) with $\mathcal{L} = 8, \mathcal{M} = 800$.

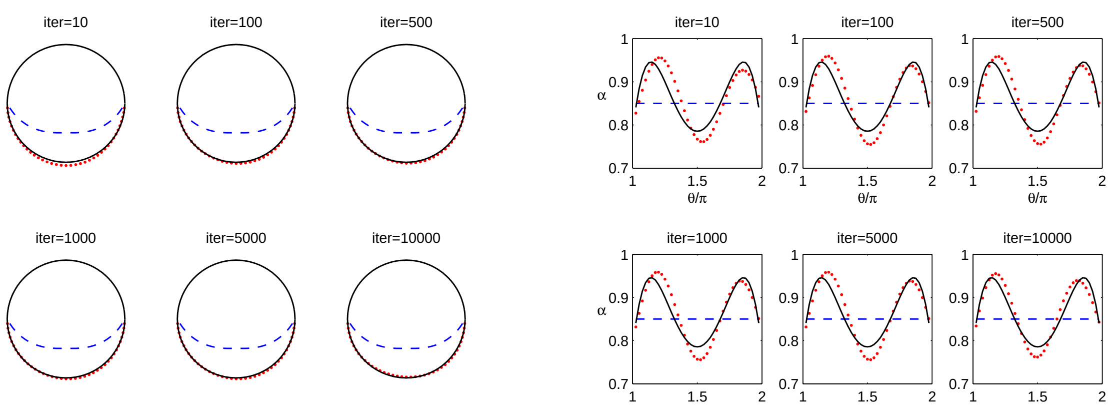

(a) (b)

FIGURE 3. Example 1: Numerically reconstructed (a) boundary Γ_2, and (b) the admittance coefficient α, for various numbers of iterations for no noise and no regularization with $M = 80, N = 40$.

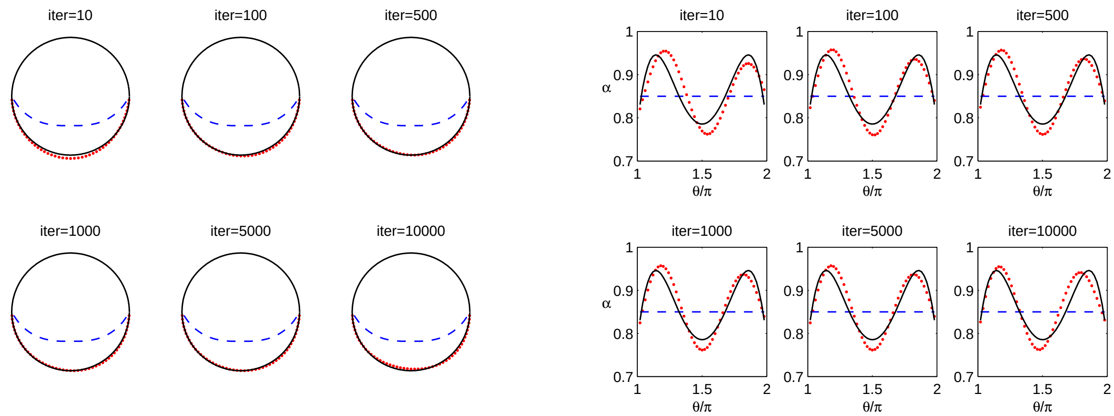

(a) (b)

FIGURE 4. Example 1: Numerically reconstructed (a) boundary Γ_2, and (b) the admittance coefficient α, for various numbers of iterations for no noise and no regularization with $M = 100, N = 50$.

We also add noise in the fluxes g_1 and g_2 as in (3.13). The numerically obtained results for noise $p = 5\%$ with $M = 80, N = 40$ and no regularization for various numbers of iterations are shown in Figure 5. From this figure we observe that as the number of iterations increases the numerical solutions for Γ_1 and especially for α become less accurate. In fact, from Figure 5(b) it can be seen that the retrieval of the admittance coefficient α when the input data is contaminated with 5% noise and no regularization is employed, is not accurate. Such a retrieval is expected because our inverse problem is ill-posed and nonlinear, hence some sort of regularization needs to be employed in order to obtain stable and accurate solutions.

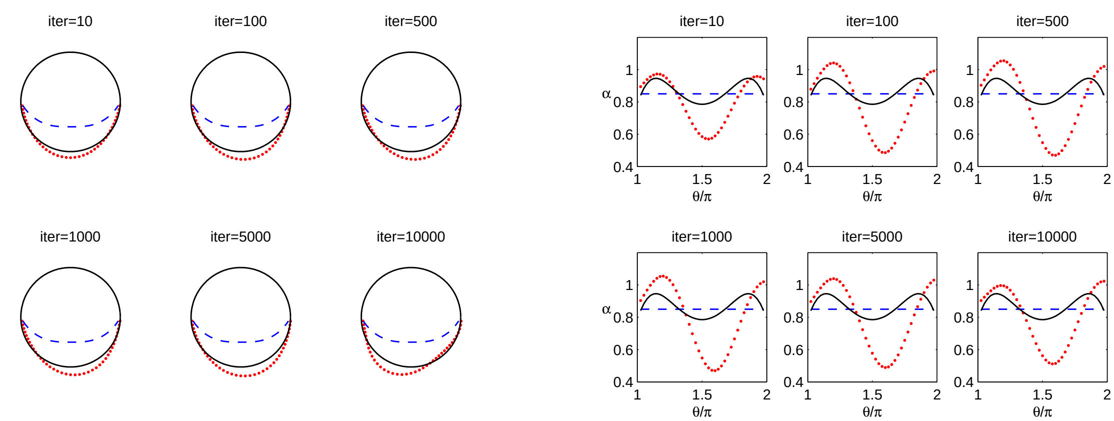

(a) (b)

FIGURE 5. Example 1: Numerically reconstructed (a) boundary Γ_2, and (b) the admittance coefficient α, for various numbers of iterations for noise $p = 5\%$ and no regularization with $M = 80, N = 40$.

The corresponding results obtained with different values of the regularization parameters λ_2 and λ_3 (λ_1 was taken to be equal to zero) after 10000 iterations are shown in Figure 6. From this figure we observe that the combination $\lambda_2 = 10^{-3}, \lambda_3 = 10^{-2}$ yields the most accurate results.

Finally, we present some results for various values of K and L in (3.10) and (3.11). In particular, in Figure 7 we present the results obtained after a maximum of 1000 iterations for no noise and no regularization with $M = 80, N = 40$ when $K = L = 5, 7, 9$ and 11. We observe that the results for the boundary Γ_2 are excellent for all choices of K and L, while slight instabilities appear in the reconstructed admittance coefficient for the cases $K = L = 5$ and 7. Of course, especially when we invert noisy data, instabilities will start to manifest as K and/or L increase and choosing appropriate values for these parameters plays the role of regularization.

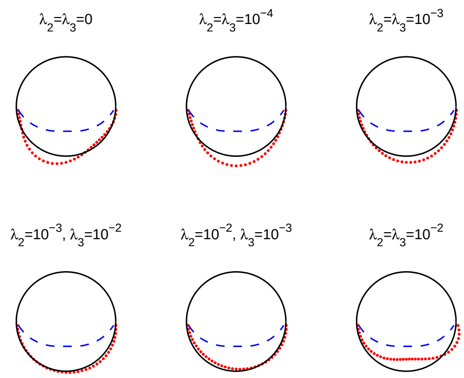

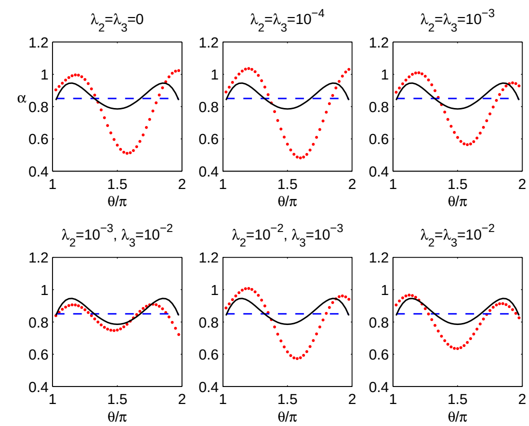

FIGURE 6. Example 1: Numerically reconstructed (a) boundary Γ_2, and (b) the admittance coefficient α, after 10000 iterations for noise $p = 5\%$ and regularization with $M = 80, N = 40$.

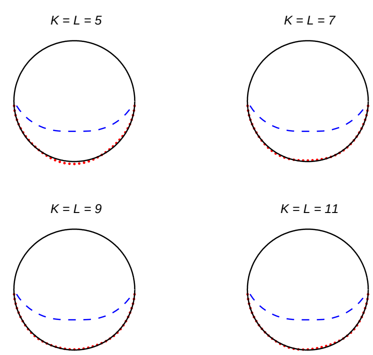

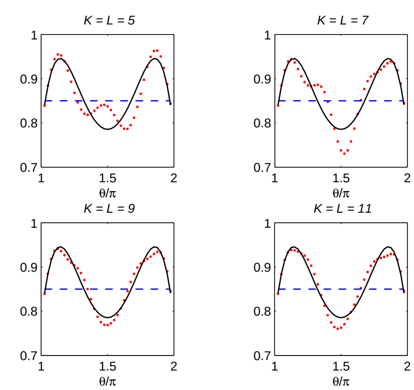

FIGURE 7. Example 1: Numerically reconstructed (a) boundary Γ_2, and (b) the admittance coefficient α, after 10000 iterations for no noise and no regularization with $M = 80, N = 40$ and $K = L = 5, 7, 9$ and 11.

4.3. **Example 2.** In this example, we consider the solution domain Ω whose boundary $\partial\Omega$ is the peanut shape defined by

$$r(\vartheta) = \sqrt{\cos^2(\vartheta) + \frac{1}{4}\sin^2(\vartheta)}, \quad \vartheta \in [0, 2\pi). \tag{4.15}$$

The boundary $\partial\Omega$ is divided into two parts, namely

$$\Gamma_1 = \{(x, y) \in \mathbb{R}^2 |\ x = r(\vartheta)\cos(\vartheta);\ y = r(\vartheta)\sin(\vartheta);\ \vartheta \in [0, \pi]\}, \tag{4.16}$$

and

$$\Gamma_2 = \{(x, y) \in \mathbb{R}^2 |\ x = r(\vartheta)\cos(\vartheta);\ y = r(\vartheta)\sin(\vartheta);\ \vartheta \in (\pi, 2\pi)\}. \tag{4.17}$$

This is a more complicated non-convex geometry to be reconstructed and hence a more severe test example than Example 1. Also, unlike Example 1, no exact solution is available for the inverse problem in the peanut shaped domain, so we construct solutions u_1 and u_2 following the technique presented in Section 4.1. For u_1 we take (4.1) with $\mathcal{A} = 1/2, \mathcal{B} = \mathcal{C} = 0$ and $\mathcal{L} = 8$, while for u_2 we take (4.1) with $\mathcal{A} = \mathcal{C} = 1, \mathcal{B} = 0$ and $\mathcal{L} = 8$. The unknown coefficients $(A_\ell)_{\ell=2}^{8}$, $(B_\ell)_{\ell=2}^{8}$ are determined by collocating equation (4.8) with $\mathcal{M} = 800$. The Dirichlet boundary data (2.6) generated in this way are linearly independent with at least one positive, see Figure 8.
The values of K, L, S and the initial guesses for the unknown vector $(\boldsymbol{c}^1, \boldsymbol{c}^2, \boldsymbol{r}, \boldsymbol{\alpha}, \eta)$ are the same as in Example 1.

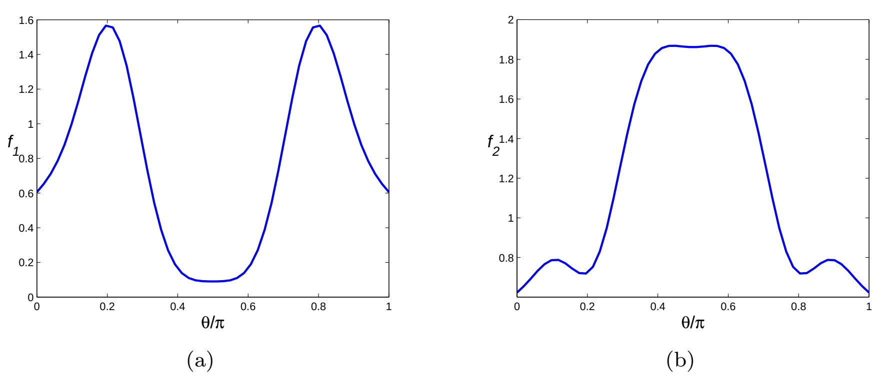

FIGURE 8. Example 2: The Dirichlet boundary data (2.6) for (a) u_1 and (b) u_2.

In Figure 9(a) we present the initial guess and numerically reconstructed boundary Γ_2 with $M = 120, N = 60$ for various numbers of iterations, no noise and no regularization. The corresponding results for the admittance coefficient α are presented in Figure 9(b). From this figure it can be seen that for exact data the numerical solutions for both Γ_2 and α converge to their exact values, as the number of iterations increases. Furthermore, no regularization was necessary.

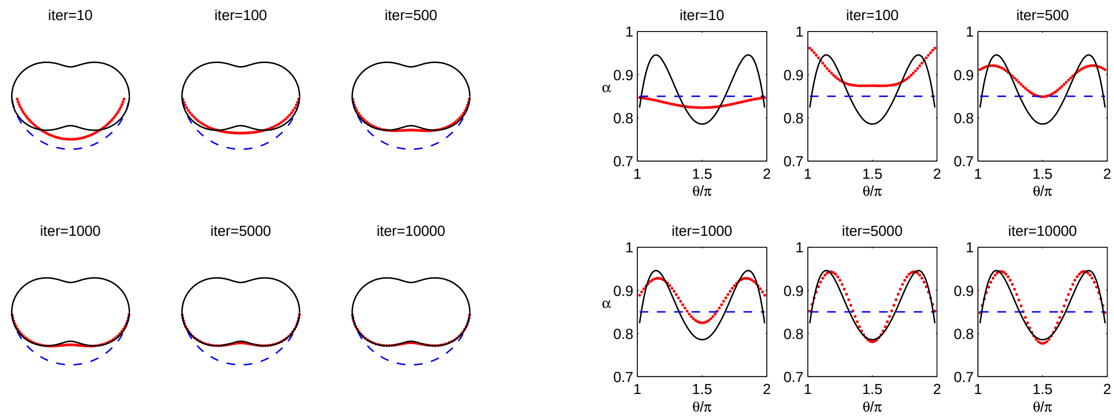

(a) (b)

FIGURE 9. Example 2: Numerically reconstructed (a) boundary Γ_2, and (b) the admittance coefficient α, for various numbers of iterations for no noise and no regularization with $M = 120, N = 60$.

The numerically obtained results for noise $p = 3\%$ added to the fluxes g_1 and g_2 in (3.13) with no regularization and $M = 120, N = 60$ for various numbers of iterations are shown in Figure 10. As in Figure 5 for Example 1, the unregularised numerical results for Γ_2 seem reasonably stable and accurate, whilst the retrieval of accurate numerical results for α is more difficult.

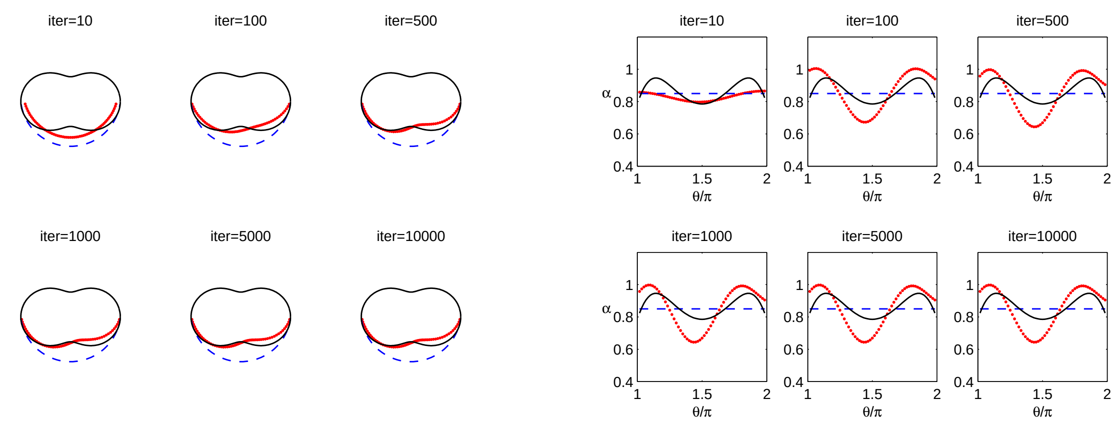

(a) (b)

FIGURE 10. Example 2: Numerically reconstructed (a) boundary Γ_2, and (b) the admittance coefficient α, for various numbers of iterations for noise $p = 3\%$ and no regularization with $M = 120, N = 60$.

The corresponding results obtained with different values of the regularization parameter λ_3 (λ_1 and λ_2 were taken to be equal to zero) after 10000 iterations are shown in Figure 11. From this figure we observe that for λ_3 between 2×10^{-3} and 10^{-2} we obtain improved results.

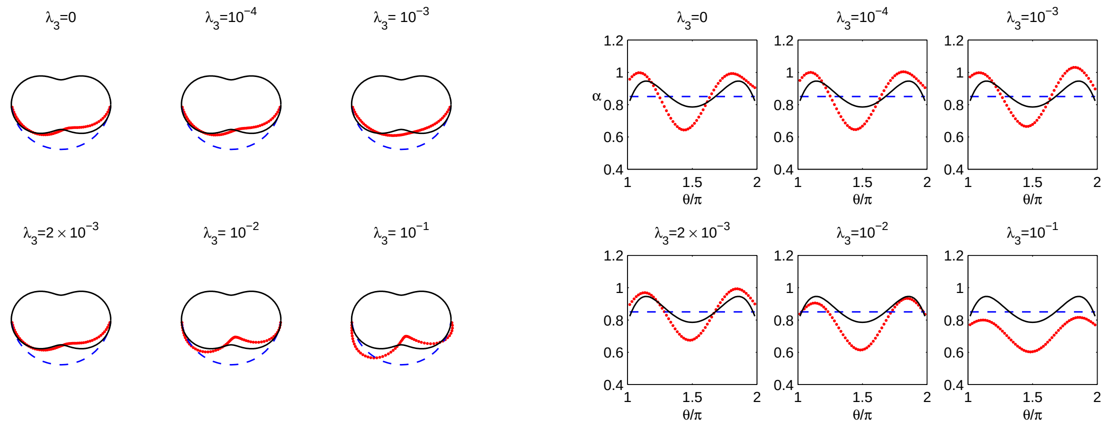

(a) (b)

FIGURE 11. Example 2: Numerically reconstructed (a) boundary Γ_2, and (b) the admittance coefficient α, after 10000 iterations for noise $p = 3\%$ and regularization with $M = 120, N = 60$.

4.4. **Example 3.** We finally consider the test example of [10] involving an apple-shaped contour $\partial\Omega$ defined by

$$r(\vartheta) = \frac{1 + 0.8\cos(\vartheta) + 0.2\sin(2\vartheta)}{1 + 0.8\cos(\vartheta)}, \quad \vartheta \in [0, 2\pi), \tag{4.18}$$

with sub-boundaries Γ_1 and Γ_2 given by (4.16) and (4.17), respectively. We generate the Cauchy data (2.6) and (2.7) in the same way as in Example 2. In particular, for u_1 we take (4.1) with $\mathcal{A} = 1/2, \mathcal{B} = \mathcal{C} = 0$ and $\mathcal{L} = 8$, while for u_2 we take (4.1) with $\mathcal{A} = \mathcal{C} = 1, \mathcal{B} = 0$ and $\mathcal{L} = 8$. The unknown coefficients $(A_\ell)_{\ell=2}^{8}$, $(B_\ell)_{\ell=2}^{8}$ are determined by collocating equation (4.8) with $\mathcal{M} = 800$. The Dirichlet boundary data (2.6) generated in this way are linearly independent with at least one positive, see Figure 12. We also take the admittance function $\alpha(\vartheta)$ to be retrieved to be the same as in Examples 1 and 2. The values of K, L, S and the initial guesses for the unknown vector $(\boldsymbol{c}^1, \boldsymbol{c}^2, \boldsymbol{r}, \boldsymbol{\alpha}, \eta)$ are the same as in Examples 1 and 2.
The numerically obtained results for noise $p = 5\%$ added to the fluxes g_1 and g_2 in (3.13) with no regularization and $M = 100, N = 50$ for various numbers of iterations are shown in Figure 13. As in the corresponding figures for Examples 1 and 2, the unregularised numerical results for Γ_2 seem reasonably stable and accurate whilst the retrieval of accurate numerical results for α is more difficult. The corresponding results obtained with different values of the regularization parameter λ_1 (λ_2 and λ_3 were taken to be equal to zero) after 10000 iterations are shown in Figure 14. From this figure we observe that for λ_1 between 10^{-5} and 10^{-4} we obtain improved results.

5. CONCLUSIONS

In this paper, the inverse geometric problem in corrosion engineering which consists of simultaneously determining an unknown portion of the boundary Γ_2 and its Robin admittance coefficient from two linearly independent pairs of Cauchy data on the known boundary $\Gamma_1 = \partial\Omega \backslash \Gamma_2$, has been investigated using the MFS. More precisely, a nonlinear regularized MFS is used in order to obtain stable and accurate numerical results for the ill-posed inverse problem in question. Clearly, the ill-posedness requires regularization in order to achieve stability. In this study, this has been achieved by adopting the finite-dimensional parametrisations (3.10) and (3.11) for Γ_2 and α, respectively, as well as the incorporation of the regularization terms (3.14) into the nonlinear least-squares functional (3.12). Numerical results show satisfactory reconstructions for the corroded boundary and its admittance coefficient with reasonable stability against noisy data. The choice of the regularization parameters $K, L, \lambda_1, \lambda_2$ and λ_3 was based on trial and error, but it is expected that more sophisticated choices [2, 13] will lead to even better reconstructions. Future work will consider extending the numerical method developed in this study to a similar inverse geometric problem with a generalized impedance boundary condition, [5, 8].

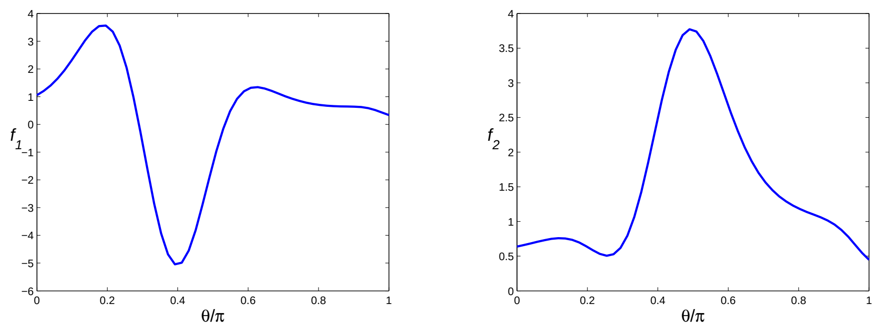

(a) (b)

Figure 12. Example 3: The Dirichlet boundary data (2.6) for (a) u_1 and (b) u_2.

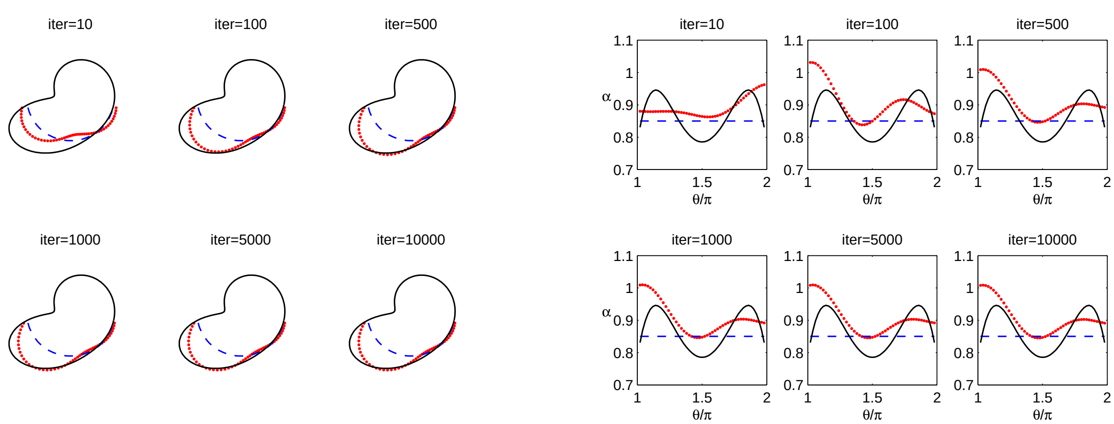

(a) (b)

Figure 13. Example 3: Numerically reconstructed (a) boundary Γ_2, and (b) the admittance coefficient α, for various numbers of iterations for noise $p = 5\%$ and no regularization with $M = 100, N = 50$.

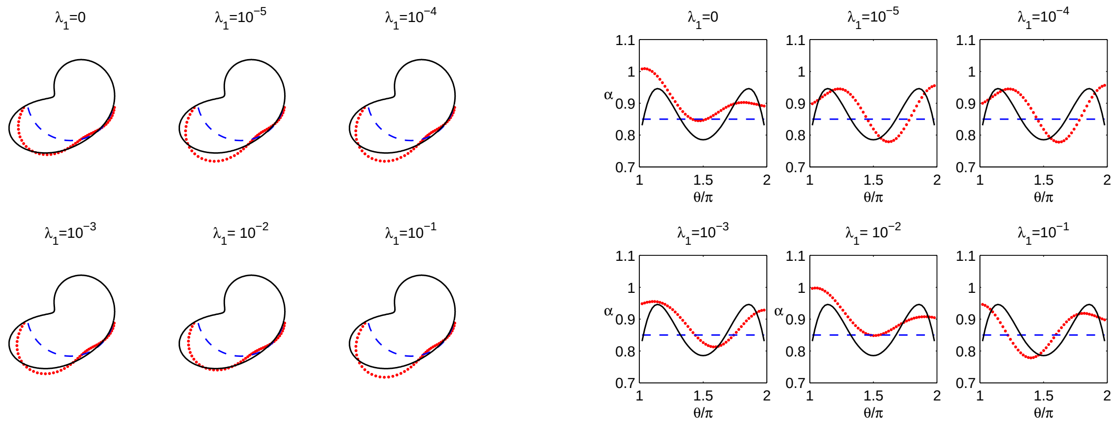

(a) (b)

FIGURE 14. Example 3: Numerically reconstructed (a) boundary Γ_2, and (b) the admittance coefficient α, after 10000 iterations for noise $p = 5\%$ and regularization with $M = 100, N = 50$.

Acknowledgements

The authors extend their appreciation to the Deanship of Scientific Research at King Saud University for funding this work through research project no. NFG-14-03-23. The support of the Universities of Cyprus, Leeds and Bucharest is also gratefully acknowledged.

References

[1] V. Bacchelli (2009) *Uniqueness for the determination of unknown boundary and impedance with homogeneous Robin condition*, Inverse Problems, **25**, 015004 (4pp).

[2] M. Belge, M.E. Kilmer and E.L. Miller (2002) *Efficient determination of multiple regularization parameters in a generalized L-curve framework*, Inverse Problems, **18**, 1161-1183.

[3] B. Bin-Mohsin and D. Lesnic (2012) *Identification of a corroded boundary and its Robin coefficient*, East Asian J. Appl. Math., **2**, 126-149.

[4] L. Bourgeois and H. Haddar (2010) *Identification of generalized impedance boundary conditions in inverse scattering problems*, Inverse Problems and Imaging, **4**, 19-38.

[5] L. Bourgeois, N. Chaulet and H. Haddar (2012) *On simultaneous identification of the shape and generalized impedance boundary condition in obstacle scattering*, SIAM J. Sci. Comput., **34**, A1824-A1848.

[6] E. Cabib, D. Fasino and E. Sincich (2011) *Linearization of a free boundary problem in corrosion detection*, J. Math. Anal. Appl., **378**, 700-709.

[7] F. Cakoni and R. Kress (2007) *Integral equations for inverse problems in corrosion detection from partial Cauchy data*, Inverse Problems and Imaging, **1**, 229-245.

[8] F. Cakoni and R. Kress (2013) *Integral equations methods for the inverse obstacle problems with generalized impedance boundary condition*, Inverse Problems, **29**, 015005 (19 pp).

[9] F. Cakoni, R. Kress and C. Schuft (2010) *Integral equations for shape and impedance reconstruction in corrosion detection*, Inverse Problems, **26**, 095012 (24pp).

[10] F. Cakoni, R. Kress and C. Schuft (2010) *Simultaneous reconstruction of the shape and impedance in corrosion detection*, Methods and Applications of Analysis, **17**, 357-378.

[11] S. Chaabane and M. Jaoua (1999) *Identification of Robin coefficients by means of boundary measurements*, Inverse Problems, **15**, 1425-1438.

[12] K. Chaji, M. El Bagdouri and R. Channa (2008) *A 2-D domain boundary estimation*, J. Phys. Conf. Ser., **135**, 012029.

[13] Z. Chen, Y. Lu, Y. Xu and H. Yang (2008) *Multi-parameter Tikhonov regularization for linear ill-posed operator equations*, J. Comput. Math., **26**, 37-55.

[14] G. Fairweather and A. Karageorghis (1998) *The method of fundamental solutions for elliptic boundary value problems*, Adv. Comput. Math., **9**, 69-95.

[15] W. Fang and S. Zeng (2009) *Numerical recovery of Robin boundary from boundary measurements for the Laplace equation*, J. Comput. Appl. Math., **224**, 573-580.
[16] G. Inglese (1997) *An inverse problem in corrosion detection*, Inverse Problems, **13**, 977-994.
[17] G. Inglese and F. Mariani (2004) *Corrosion detection in conducting boundaries*, Inverse Problems, **20**, 1207-1215.
[18] V. Isakov (2009) *Inverse obstacle problems*, Inverse Problems, **25**, 123002 (18pp).
[19] A. Karageorghis, D. Lesnic and L. Marin (2011) *Survey of applications of the MFS to inverse problems*, Inverse Problems Sci. Eng., **19**, 309-336.
[20] A. Karageorghis, D. Lesnic and L. Marin (2013) *A moving pseudo-boundary MFS for void detection*, Numer. Meth. Partial Differential Equations, **29**, 935-960.
[21] A. Karageorghis, D. Lesnic and L. Marin (2013) *A moving pseudo-boundary MFS for three-dimensional void detection*, Adv. Appl. Math. Mech., **5**, 510-527.
[22] P. Kaup and F. Santosa (1995) *Nondestructive evaluation of corrosion damage using electrostatic boundary measurements*, J. Nondestructive Evaluation, **14**, 309-336.
[23] R. Kress (2001) *A Nyström method for boundary integral equations in domains with corners*, Numer. Math., **58**, 145-161.
[24] R. Kress and W. Rundell (2001) *Inverse scattering for shape and impedance*, Inverse Problems, **17**, 1075-1085.
[25] W.H. Loh (1987) *Modeling and Measurement of Contact Resistances*, Stanford Electronics Labs., Technical Report G830-1.
[26] L. Marin (2009) *Boundary reconstruction in two-dimensional functionally graded materials using a regularized MFS*, CMES Comput. Model. Eng. Sci., **46**, 221-253.
[27] L. Marin and A. Karageorghis (2009) *Regularized MFS-based boundary identification in two-dimensional Helmholtz-type equations*, CMC Comput. Mater. Continua, **10**, 259-293.
[28] L. Marin, A. Karageorghis and D. Lesnic (2011) *The MFS for numerical boundary identification in two-dimensional harmonic problems*, Eng. Anal. Boundary Elements, **35**, 342-354.
[29] L. Marin and L. Munteanu (2010) *Boundary identification in two-dimensional steady state anisotropic heat conduction using a regularized meshless method*, Int. J. Heat Mass Transfer, **53**, 5815-5826.
[30] N. F. M. Martins, On the identification of perfectly conducting or insulating inclusions from one single boundary measurement, in O. Fudym, J.-L. Battaglia, G.S. Dulikravich, H.R.B. Orlande and M.J. Colaco, Editors, *4th Inverse Problems, Design and Opimization Symposium (IPDO 2013)*, Ecole des Mines d'Albi-Carmaux, Albi, France, 2013, Paper **06397** (10 pages).
[31] The MathWorks, Inc., 3 Apple Hill Dr., Natick, MA, *Matlab*.
[32] N. Mera and D. Lesnic (2005) *A three-dimensional boundary determination problem in potential corrosion damage*, Comput. Mech., **36**, 129-138.
[33] Numerical Algorithms Group Library Mark 21, NAG(UK) Ltd, Wilkinson House, Jordan Hill Road, Oxford, UK (2007).
[34] C.D. Pagani and D. Pierotti (2009) *Identifiability problems and defects with the Robin condition*, Inverse Problems, **25**, 055007 (12pp).
[35] W. Rundell (2008) *Recovering an obstacle and its impedance from Cauchy data*, Inverse Problems, **24**, 045003 (22pp).
[36] E. Sincich (2010) *Stability for the determination of unknown boundary and impedance with a Robin boundary condition*, SIAM J. Math. Anal., **42**, 2922-2943.
[37] F.L. Yang, L. Yan and T. Wei (2009) *Reconstruction of part of boundary for the Laplace equation by using a regularized method of fundamental solutions*, Inverse Problems Sci. Eng., **17**, 1113-1128.

Department of Mathematics and Statistics, University of Cyprus/ Πανεπιστημιο Κυπρου, P.O.Box 20537, 1678 Nicosia/Λευκωσια, Cyprus/Κυπρος
E-mail address: `andreask@ucy.ac.cy`

Department of Mathematics, King Saud University, P. O. Box 4341, Riyadh 11491, Saudi Arabia
E-mail address: `almohsin.bandar@gmail.com`

Department of Applied Mathematics, University of Leeds, Leeds LS2 9JT, UK
E-mail address: `amt5ld@maths.leeds.ac.uk`

Department of Mathematics, Faculty of Mathematics and Computer Science, University of Bucharest, 14 Academiei, 010014 Bucharest, Romania, and Institute of Solid Mechanics, Romanian Academy, 15 Constantin Mille, 010141 Bucharest, Romania
E-mail address: `marin.liviu@gmail.com; liviu.marin@fmi.unibuc.ro`